*energies*

MDPI

*Article*

# Non-Intrusive Arc Fault Detection and Localization Method Based on the Mann–Kendall Test and Current Decomposition

**Wenqian Jiang [1,2], Bo Liu [1,*], Zhou Yang [2], Hanju Cai [1], Xiuqing Lin [2] and Da Xu [1]**

[1] School of Electrical and Information Engineering, Tianjin University, Tianjin 300072, China; jwqqsky@126.com (W.J.)
[2] Measurement Center of Guangxi Power Grid Co., Ltd., Nanning 530023, China
* Correspondence: liubo@tju.edu.cn

**Abstract:** In recent years, electrical fires caused by arc faults have been increasing, seriously affecting the safety of people's lives and property. Considering the complex arc fault characteristics of actual low-voltage users, the non-intrusive arc fault detection and localization method is studied. First, the characteristics of arc current waveforms are analyzed, and event detection based on the Mann–Kendall Test is performed for the difference between the current waveforms of two adjacent cycles, rather than using the current waveforms directly. Then, the current waveforms of the two segments are calculated via subtraction to obtain the current waveform of the electric appliances causing the event. A current feature parameter database of the normal and arc currents is constructed via harmonic analysis, and a multi-appliance current decomposition model considering the sparse operation characteristics of appliances is established; thus, the arc localization problem is transformed into an optimization problem. Finally, a genetic algorithm is used to optimize the differential current decomposition results, and then, locate the arc fault. A household arc fault simulation experiment is carried out for the common electric appliances of actual low-voltage users. The experimental results show that the proposed non-intrusive arc fault detection and localization method is effective.

**Keywords:** arc fault detection and localization; series arc; non-intrusive; Mann–Kendall Test; current disaggregation

check for updates

**Citation:** Jiang, W.; Liu, B.; Yang, Z.; Cai, H.; Lin, X.; Xu, D. Non-Intrusive Arc Fault Detection and Localization Method Based on the Mann–Kendall Test and Current Decomposition. *Energies* **2023**, *16*, 3988. https://doi.org/10.3390/en16103988

Academic Editor: Igor Timoshkin

Received: 23 March 2023
Revised: 22 April 2023
Accepted: 3 May 2023
Published: 9 May 2023

**Copyright:** © 2023 by the authors. Licensee MDPI, Basel, Switzerland. This article is an open access article distributed under the terms and conditions of the Creative Commons Attribution (CC BY) license (https://creativecommons.org/licenses/by/4.0/).

## 1. Introduction

With the development of society, people's electricity consumption has increased greatly. As a result, a large number of electrical fires occur frequently, causing huge economic losses and casualties, which seriously threatens the safety of people's lives and property [1]. Long-term overload operation or poor electrical connections, aging electrical lines or equipment insulation layers and the breakdown of the insulation medium can all lead to arc faults [2]. The power supply lines of modern buildings are usually located inside the walls and floors, and electrical equipment such as lighting fixtures and central air conditioners are also embedded in the decoration boards, which brings great difficulty to the maintenance and detection of wires, making them electrical fire hazards. When an arc fault occurs, the temperature of the fault point will reach thousands of degrees Celsius [3], melt the surrounding metal and ignite nearby combustibles, causing electrical fires, and may even involve other lines, leading to large-scale blackouts of regional power distribution systems, explosions and other serious incidents. A large number of studies show that arc faults in low-voltage distribution lines are the main cause of electrical fires. Therefore, it is of great significance to study the detection and localization methods of arc faults in low-voltage distribution systems.

The hidden danger of arc faults may be distributed in the whole low-voltage distribution system. Arc faults can be divided into three types: series arc faults, parallel arc faults and ground arc faults [4,5]. Parallel arc faults will lead to an increase in the main circuit

current, and the fault current of a grounding arc fault flows from the wire to the earth, forming a leakage current loop. Therefore, these two types of arc faults are easily detected by traditional protection devices. A series arc is equivalent to a nonlinear resistive component, and a arc in series with the load will lead to an increase in the total load impedance in the main circuit. When a series arc fault occurs, the current in the circuit is less than the load current under normal operation, and there is no ground leakage current, which makes it difficult or impossible for the traditional circuit breaker or fuse to operate [6,7].

At present, to solve the problem of how to detect series arc faults, many scholars mainly study the following three aspects: The first is based on mathematical models that describe dynamic changes in the series arc through mathematical equations, including the Cassie model [8], the Mayr model [9] and various models that improve upon them [10–15]. Due to the randomness and aperiodicity of series arc faults, there are no arc mathematical models that can accurately describe the current waveforms of the series arc faults under various working conditions. Therefore, the methods based on mathematical models mostly stay in the simulation stage. The second aspect is based on the arc's physical characteristics, such as arc light, sound, electromagnetic radiation, etc. [16–18]. This type of detection methods use advanced sensing technology to realize intelligent diagnosis of the series arc fault. Because the installation position of the detection sensor is fixed, it is only suitable for detecting series arc faults in a fixed position. The third aspect is based on arc voltage and current characteristics, and is the mainstream research direction of series arc fault detection. When an arc occurs, the electrical signal waveforms will be more distorted. Arc fault detection can be achieved by extracting appropriate features and comparing them with normal values. Commonly used features include time domain characteristics such as current fluctuation features and zero-current feature [19]; inter-period correlations between the current [20], current average and current pole difference [21]; the current amplitude spectrum [22]; the symmetry of the voltage waveform [23]; sparse coding [24], etc. In addition, some studies deal with the current signal using signal analysis methods to obtain the feature vector and construct the mapping relationship between the feature vector and the series arc fault. By inputting the feature vector into the classifier, such as a support vector machine [25], a convolutional neural network [26], a recurrent neural network [27], random forest [28], etc., an arc fault identification model is established. Commonly used signal analysis methods include Fourier transform [29], Chirp Z-Transform [30], wavelet transform [31], empirical mode decomposition [32], etc. However, it is difficult to extract common features of loads and determine the feature thresholds of different loads. In addition, most of the existing methods can only judge whether there is a series arc fault in simple load scenarios, and it is difficult to detect in complex scenarios. The arc fault detection equipment needs to be deployed on the socket of each electric appliance, which is difficult to implement in reality. Few methods can directly realize arc fault detection, identification and localization at the entrance of the user 's residential power supply. Reference [33] proposes an arc feature extraction method suitable for complex scenarios, and it was proven that the features extracted from the aggregated current can be used to identify electric appliances that produce an arc fault. In reference [34], a non-intrusive arc fault detection and localization method is proposed. A current waveform database of normal and arc fault electric appliances is constructed, and the aggregated current at the power supply entrance is decomposed in real time to detect and locate the arc faults. Reference [35] proposes a two-step method for series arc fault detection and localization, based on the $MVC_{50}$ feature vector, but it is difficult to collect the arc voltage signal using this method, and it is prone to wrong localization for the same types of electric appliances.

In this paper, in order to improve the calculation speed and the accuracy of non-intrusive series arc fault detection, a novel non-intrusive series arc fault detection and localization method based on the Mann–Kendall Test and current decomposition is proposed. The event is detected in terms of current waveform change, and then, the differential current before and after the event is obtained. The differential current is decomposed to detect and locate the arc. The main contributions are as follows:

- A current event detection method is proposed. For the first time, we introduce the Mann–Kendall Test for series arc fault detection. The difference in current waveforms between two adjacent cycles is used instead of using current data directly for event detection. The differential current is decomposed only after the event is detected, which improves computational efficiency.
- A non-intrusive arc detection and localization model based on differential current decomposition is constructed. The decomposition of the differential current can not only accelerate the operation speed, but also takes into account situations wherein multiple electric appliances change their states at the same time, which reduces false positives.
- The method is verified in physical experiment scenarios. In order to realize the non-intrusive detection of arc faults in complex scenarios, a physical arc fault experimental platform is built to collect aggregated current and terminal voltage data when multiple electric appliances are running at the same time, and the practicability of the proposed method is verified.

The rest of this paper is organized as follows: In Section 2, the current event detection method based on the Mann–Kendall Test is introduced. On this basis, In Section 3, a calculation method for differential currents is proposed and the current decomposition model proposed in this paper is introduced in detail. Section 4 introduces the framework of this method. Then, the experimental results are presented and analyzed in Section 5. Finally, Section 6 summarizes the paper.

## 2. Current Event Detection Method

### *2.1. Analysis of Arc Current Characteristics*

In order to analyze the characteristics of arc faults and construct a sample database of series arc faults in common electric appliances, we built a physical arc fault generator, which can generate series arc faults under various appliances' operating conditions, and record the arc fault current waveform. Figure 1 is a schematic diagram of arc fault current waveform data acquisition, in which the arc fault generator is built according to the UL1699 standard [36]. The arc generator consists of a movable electrode and a fixed electrode. The arc current waveforms are generated by connecting different appliances and controlling the gap between the two electrodes.

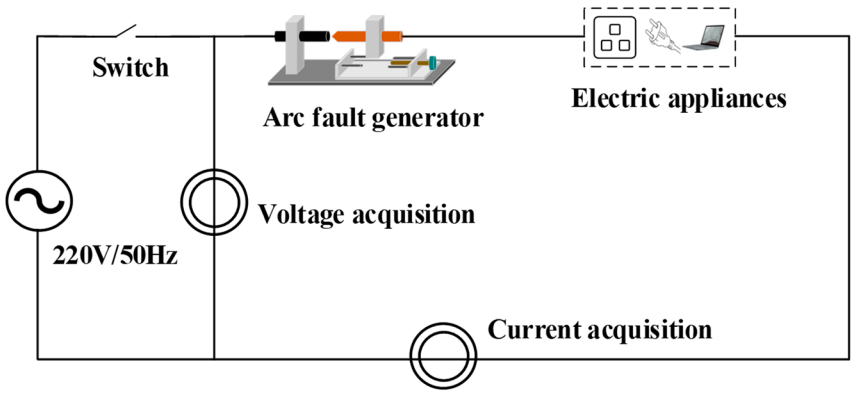



**Figure 1.** Schematic diagram of arc fault data acquisition.

In the household, there are a variety of electric appliances that can usually be divided into the following types: resistive appliances, inductive appliances and appliances with the switching power supply. In this paper, we selected three corresponding typical appliances for our research: an electric kettle, an air conditioner and a laptop, respectively. Their rated parameters are shown in Table 1. According to the above arc fault data acquisition schematic, we carried out experiments and recorded the current and voltage data of each appliance under its normal and arc fault operations. The data sampling frequency was 25 kHz. Figure 2 shows the normal current waveforms and arc fault current waveforms of

the three appliances. It should be noted that the voltage data were measured at the power supply for all appliances under different conditions, that is, 220 V/50 Hz, so the voltage waveform is not displayed in detail.

**Table 1.** Rated parameters of the three electric appliances.

| Appliances | Rated Voltage | Rated Power |
|---|---|---|
| Electric kettle | 220 V | 1800 W |
| Air conditioner | 220 V | 1300 W |
| Laptop | 220 V | 90 W |

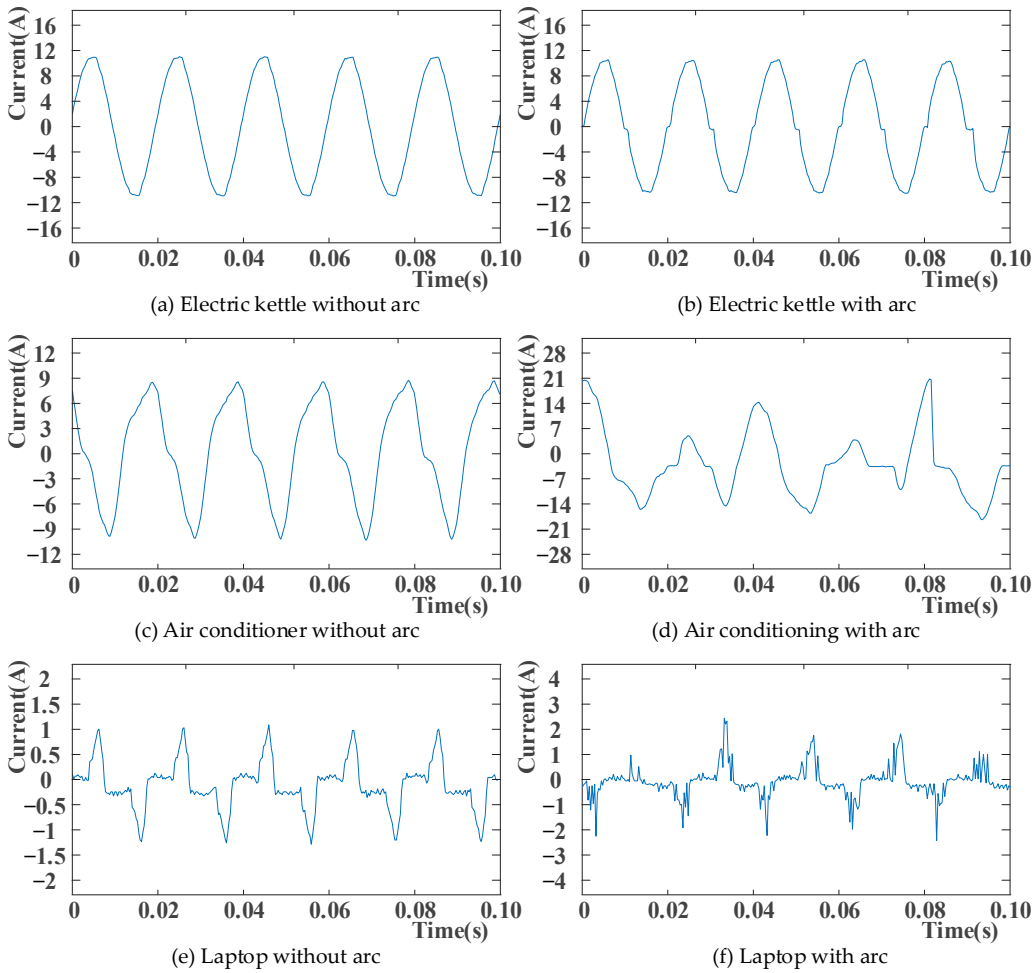



**Figure 2.** Appliance current waveforms with and without arc.

It can be seen that the current waveform is periodic when the appliance is under normal operation. However, when the arc fault occurs, the arc current of the kettle has obvious current-zero characteristics. The arc current of the air conditioner is no longer periodic, and the current waveform has a large range of distortion with different amplitudes. The arc current of the laptop fluctuates irregularly, and there are large differences between adjacent cycles. Additionally, a large number of burrs appear, and the proportion of sampling points near the zero value increases. In summary, when a series arc fault occurs, the arc current waveform has obvious characteristics. That is, there will be asymmetry of the periodic waveform, a current-zero phenomenon, a high occurrence of high-order harmonics, and a large change rate of waveforms.

### 2.2. Event Detection Method Based on the Mann–Kendall Test

At present, some scholars use time series analysis algorithms, such as approximate entropy [37] and sample entropy, to detect current events, but these algorithms are affected by parameters and window size, and the calculation time is long. Mann–Kendall Test [38] is a trend analysis method often used in hydrological, meteorological and geoscience time series to detect the time of abrupt climate change. The Mann–Kendall Test does not require the data samples to follow a certain distribution, and is not disturbed by a few outliers. It is a nonparametric time series detection method that is simple in calculation and insensitive to data boundaries. The principle of the Mann–Kendall Test is as follows:

For a time series $X$ ($x_1$, $x_2$, ... , $x_n$) with $n$ samples, a rank sequence $s_k$ is constructed:

$$s_k = \sum_{i=1}^{k} r_i, \quad (k = 2, 3, \cdots, n) \tag{1}$$

$$r_i = \begin{cases} +1 (x_i > x_j) \\ 0 (x_i \leq x_j) \end{cases} \quad j = 1, 2, \cdots, i \tag{2}$$

It can be seen that the rank sequence $s_k$ is a cumulative count of the number of values at time $i$ that are greater than the number at time $j$. Assuming that the time series is stochastically independent, we can define the statistics as follows:

$$UF_k = \frac{[s_k - E(s_k)]}{\sqrt{\mathrm{Var}(s_k)}} \quad (k = 1, 2, \cdots, n) \tag{3}$$

where $UF_1 = 0$, $E(s_k)$ and $\mathrm{Var}(s_k)$ are the mean and variance of the cumulative count $s_k$. When $x_1$, $x_2$, ... , $x_n$ are independent of each other and have the same continuous distribution, they can be calculated using the following formula:

$$E(s_k) = \frac{n(n+1)}{4}, \quad \mathrm{Var}(s_k) = \frac{n(n-1)(2n+5)}{72} \tag{4}$$

$UF_k$ is a standard normal distribution. It is a series of statistics calculated by time series $x_1$, $x_2$, ... , $x_n$.

According to the reverse order of time series $X$, that is $x_n$, ... , $x_2$, $x_1$, the above process is repeated, and $UB_k = -UF_k$, $k = n, n-l, \ldots, 1$, $UB_1, = 0$. When the $UF$ and $UB$ curves intersect at a point in the confidence interval, the time of intersection corresponds to the timestamp of time series mutation.

In this paper, the Mann–Kendall test is performed using the difference between the current waveforms of two adjacent cycles ($D_c$) rather than directly using the current time series. The calculation formula to determine the difference between the current waveforms of two adjacent cycles is as follows:

$$D_c = \frac{1}{N} \sum_{j=1}^{N} |\Delta i_k(j)| \tag{5}$$

$$\Delta i_k(j) = i_k(j) - i_{k-1}(j) \quad j = 1, 2, \cdots, N; k = 2, 3, \cdots, M \tag{6}$$

where $N$ is the number of sampling points per current cycle, the number of cycles is $M$, and the current sampling values for two adjacent cycles are $i_{k-1}$ and $i_k$, respectively.

Figure 3 shows the value of $D_c$ in some scenarios. (a)–(c) represent the $D_c$ value without and with the arc when only one single electric appliance is operating. (d) shows the $D_c$ value of the aggregated current with an arc on the common branch under the operation of multiple appliances. It can be seen that the $D_c$ values of different appliances are relatively stable at a small value under normal operation. However, when a series arc fault occurs, the magnitudes are much larger with large fluctuations. When an arc occurs, the value of

$D_c$ suddenly increases, so the Mann–Kendall test can be carried out for $D_c$, so as to obtain the timestamp of when the current changes suddenly.

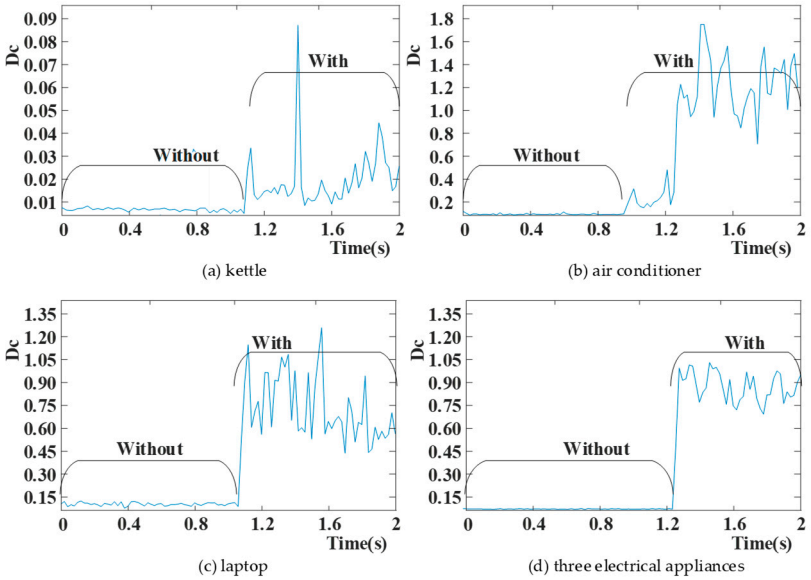



**Figure 3.** Values of $D_c$ under normal and arc fault conditions of different appliances.

According to the principle of the Mann–Kendall Test, event detection is conducted for $D_c$, which is extracted from the aggregated current measured at the power supply entrance, and the event detection results are shown in Figure 4. In this paper, the significance level for the Mann–Kendall Test is set to 0.01. By comparing Figures 3 and 4, it can be found that the errors of the event detection results are small, and the current mutation points can be accurately located. Current event detection provides a basis for differential current extraction and current decomposition in the next section.

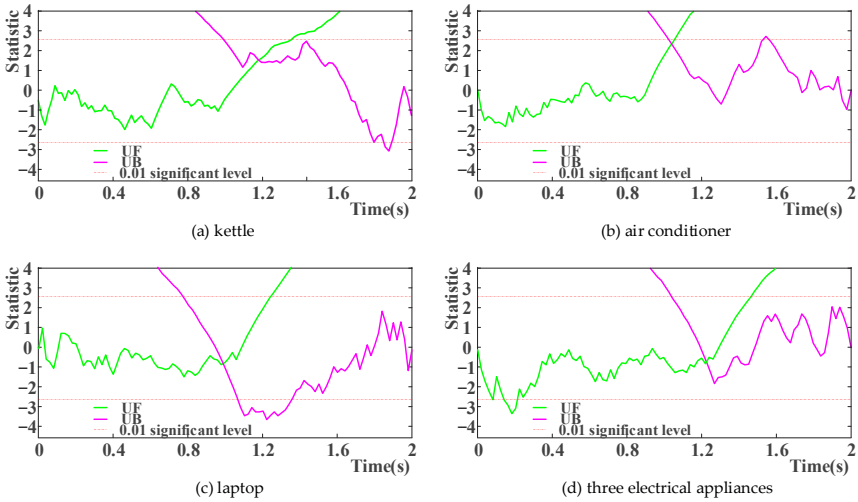
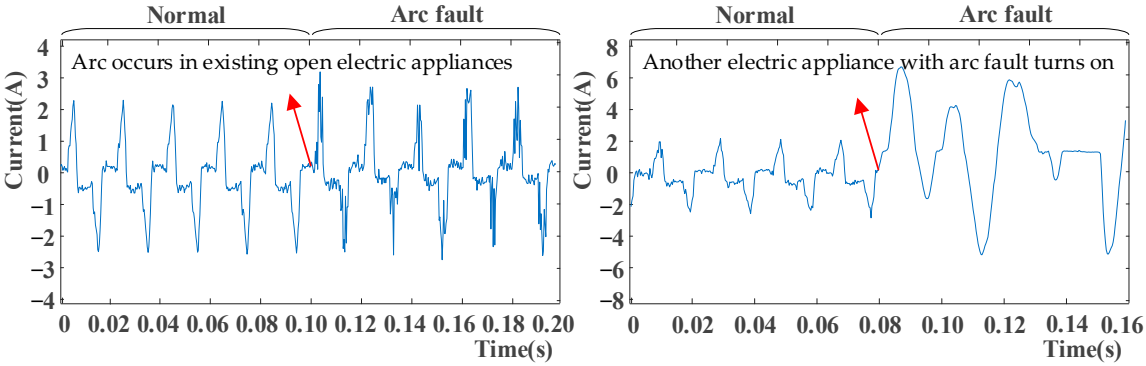



**Figure 4.** The event detection of $D_c$ in Figure 3 based on Mann–Kendall Test.

As shown in Figure 5, the sudden changes in the aggregated current can be divided into two cases: case 1 is where the electric appliance operates under normal conditions at the beginning and a sudden arc fault occurs, resulting in distortion of the current waveform; case 2 is where a certain electric appliance turns on or off, and the current suddenly increases or decreases. The event detection examples shown above belong to case 1. For case 2, when a normal electric appliance is turned on or off, the value of $D_c$ will not have a large change, so no arc event will be detected, which will not affect the arc detection. If the

branch where the switched electric appliance is located has a potential arc hazard, the $D_c$ value will suddenly increase. The event detection results in this case are similar to those in case 1 mentioned above, so we do not show them in this paper.




(a) arc fault in case 1 (b) arc fault in case 2

**Figure 5.** Two cases of arc fault occurrence.

## 3. Arc Detection and Localization Based on Differential Current Decomposition

### *3.1. Differential Current Extraction*

The aggregated current at the power supply entrance is superimposed by the current waveforms of many electric appliances in the household. If the aggregated current is directly decomposed, it is not only slow in calculation, but also prone to false detection and missed detection. Therefore, this paper proposes an arc detection and localization method based on the decomposition of the differential current, which calculates the difference in the currents before and after an event. In most cases, only one appliance changes its operating state and generates an event in a relatively short period of time, but there are also cases where multiple appliances change their operating states at the same time, such as turning on a plug socket that connects multiple appliances. So, the differential current is only the current of the appliances that generate events, and in most cases, it corresponds to a single appliance; in few cases, it is the superimposed current of multiple appliances, but generally not all of the appliances in the house. Therefore, the decomposition of the extracted differential current can not only improve detection accuracy, but also reduce calculation time.

Considering that the Mann–Kendall Test-based event detection method introduced in the previous section inevitably has some errors, we select 20 cycles before and after the mutation point, respectively, as shown in Figure 6. We divide these 40 cycles into an error elimination area and a differential calculation area, and each area includes 20 cycles. The differential current is obtained by subtracting the cycles in the differential calculation area before and after the mutation point. The differential current consists of ten current cycles.

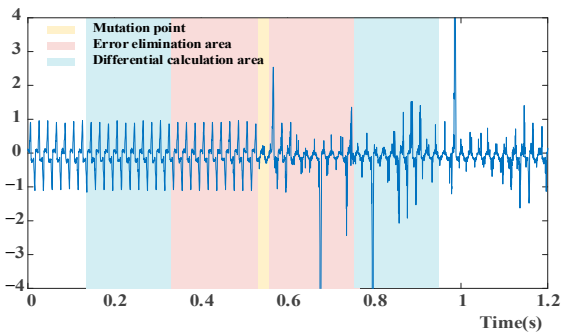



**Figure 6.** Differential current calculation diagram.

The principle of differential current calculation is as follows: firstly, find the two corresponding groups of 10 voltage waveforms in the differential calculation area. In order to ensure that the current waveforms $I_2$ and $I_1$ can be directly subtracted in the time domain, their voltage phase angles should be the same. So, we align the positive zero-crossing points of the two groups of the first voltage waveform before and after the event, and under this condition, the difference in the current before and after the event can be obtained by subtracting the corresponding current waveform values in turn. The differential current calculation formula is expressed as follows:

$$I_{event} = I_2 - I_1 \tag{7}$$

where $I_{event}$ is the differential current, $I_2$ is the current waveform selected after the event, and $I_1$ is the current waveform selected before the event.

When the event is caused by an electric appliance being turned on, that is, it belongs to case 2 mentioned in Section 2.2, the following applies:

$$I_2 = I_1 + I_{open}, \quad I_{event} = I_2 - I_1 = I_{open} \tag{8}$$

where $I_{open}$ is the current of the electric appliance being turned on.

When the event is caused by an arc fault related to the electric appliance being turned on, that is, it belongs to case 1 mentioned in Section 2.2, the following applies:

$$I_2 = I_{other} + I_{arc}, \quad I_1 = I_{other} + I_{normal} \tag{9}$$

where $I_{other}$ is the superimposed current of the appliances, other than the appliance generating the event, $I_{normal}$ is the normal current of the appliance generating the event, and $I_{arc}$ is the arc current of the appliance generating the event.

The differential current is as follows:

$$I_{event} = I_2 - I_1 = I_{arc} - I_{normal} \tag{10}$$

### *3.2. Arc Current Disaggregation and Fault Localization*

It can be seen from Figure 2 that the current waveforms are different for different electric appliances, and are also significantly different for the normal and arc states of the same appliance. Therefore, by extracting the current features of different appliances in normal and arc fault states and distinguishing them, the arc fault can be identified, as can the corresponding electric appliances. In this paper, a differential current decomposition model is proposed. By converting the arc detection problem into an optimization problem, the principle is as follows [34]:

The current of an electric appliance can be decomposed into:

$$i_a(t) = \sum_{\forall k \in N^*} \alpha_{k,a} \bullet \cos(k\omega t + \theta_{k,a}) \tag{11}$$

where $i_a(t)$ is the appliance current, $a$ represents the appliance, $k$ = 1, 2, . . . , $k\omega$ represents the angular frequency of the *kth* harmonic component in the current, $\alpha_{k,a}$ is the amplitude of the *kth* harmonic content, and $\theta_{k,a}$ represents the initial phase angle of the *k-th* harmonic component.

The model in (11) can be used to describe the current waveform generated by any appliance under a certain operating state. However, under actual working conditions, the aggregated current often contains $m$ different appliances. At this time, the aggregated current can be approximately estimated through the linear superposition of the $m$ appliances' currents:

$$I(t) = \sum_{a=1}^{m} \left( \delta_a \bullet i_a(t) + \beta_a \bullet i'_a(t) \right) \tag{12}$$

where $i_a(t)$ and $i'_a(t)$ are the current waveforms generated by the appliance $a$ under normal and arc fault conditions, respectively, $\delta \in \{0,1,-1\}$ and $\beta \in \{0,1,-1\}$ are the operating state parameters of each appliance, and $-1 \leq \delta_a + \beta_a \leq 1$ for any appliance. Additionally, if $\delta_a = -1$, then $\beta_a = 1$.

Let $\boldsymbol{\delta} = [\delta_1, \delta_2, \ldots, \delta_m]$ and $\boldsymbol{\beta} = [\beta_1, \beta_2, \ldots, \beta_m]$. According to Formula (11), (12) is expressed in matrix form as follows:

$$\begin{bmatrix} \alpha_{1,I}\angle\theta_{1,I} \\ \alpha_{2,I}\angle\theta_{2,I} \\ \vdots \\ \alpha_{k,I}\angle\theta_{k,I} \end{bmatrix} = \begin{bmatrix} \alpha_{1,1}\angle\theta_{1,1} & \cdots & \alpha_{1,m}\angle\theta_{1,m} & \alpha'_{1,1}\angle\theta'_{1,1} & \cdots & \alpha'_{1,m}\angle\theta'_{1,m} \\ \alpha_{2,1}\angle\theta_{2,1} & \cdots & \alpha_{2,m}\angle\theta_{2,m} & \alpha'_{2,1}\angle\theta'_{2,1} & \cdots & \alpha'_{2,m}\angle\theta'_{2,m} \\ \vdots & \cdots & \vdots & \vdots & \cdots & \vdots \\ \alpha_{k,1}\angle\theta_{k,1} & \cdots & \alpha_{k,m}\angle\theta_{k,m} & \alpha'_{k,1}\angle\theta'_{k,1} & \cdots & \alpha'_{k,m}\angle\theta'_{k,m} \end{bmatrix} \begin{bmatrix} \boldsymbol{\delta}^T \\ \boldsymbol{\beta}^T \end{bmatrix} \tag{13}$$

where $m$ is the number of electric appliances in operation. Since $I(t)$ is the measured aggregated current, $\alpha_{k,I}$ and $\theta_{k,I}$ are known quantities, and they are the amplitude and phase angle of the *kth* harmonic of the aggregated current, respectively, which can be obtained via online measurement; $\alpha_{k,m}$, $\alpha'_{k,m}$, $\theta_{k,m}$ and $\theta'_{k,m}$ are the amplitude and phase angle of the *kth* harmonic of the electric appliance $m$ under normal operation and arc fault, respectively, and they can be obtained based on experiments. So, only $\boldsymbol{\delta}$ and $\boldsymbol{\beta}$ are unknown. Equation (13) can be simplified as $\boldsymbol{I} = \mathbf{A} \bullet \boldsymbol{H}$; $\mathbf{A}$ is the current feature parameter matrix, which contains the current waveform information of each appliance under the normal operation and arc fault states. Additionally, $\boldsymbol{H} = (\boldsymbol{\delta}, \boldsymbol{\beta})^{\mathrm{T}}$ is the state coefficient matrix, which represents the different operating states of each appliance. Then, the following optimization objective function can be established:

$$\min_{H} \|\boldsymbol{I} - \mathbf{A} \bullet \boldsymbol{H}\|_2 \tag{14}$$

where $\|\bullet\|_2$ is the 2-norm, and $\boldsymbol{H}$ is the unknown vector to be solved.

In order to further improve the decomposition accuracy, according to practical experience, the sparsity characteristics of appliance operations are integrated into the decomposition model. Sparsity means that when the measured aggregated current could correspond to multiple appliance combinations within an acceptable error range, it prefers to fit the measured values with a combination of a smaller number of appliances, since we use the differential current for decomposition. In this way, it can avoid overfitting optimization of the decomposition model (for example, when the model database contains six resistive loads ($Q_1$, $Q_2$, $Q_3$, $Q_4$, $Q_5$, and $Q_6$), where $I_{Q1}$ = 10A, $I_{Q2}$ = 8A, $I_{Q3}$ = 6A, $I_{Q4}$ = 5A, and $I_{Q5}$ = 4A, $I_{Q6}$ = 3A. When the actual differential current is 18 A and the harmonic content is almost zero, the decomposition result after adding the sparsity characteristic is $I_{Q1}$, $I_{Q2}$, rather than $I_{Q3}$, $I_{Q4}$, $I_{Q5}$, $I_{Q6}$. This is because in reality, the probability of opening four electric appliances at the same time is very small). Although this characteristic is not always satisfied in all scenarios, according to the actual test in the existing appliances database, adding this feature can achieve good results.

In this paper, we use $\|\boldsymbol{H}\|_1$, which is the number of 1 in the state coefficient vector $\boldsymbol{H}$ to characterize the appliance sparsity, where $\|\bullet\|_1$ is the 1-norm. We add $\|\boldsymbol{H}\|_1$ to the objective function in the form of a penalty term, aiming to find appliance combinations that are more in line with engineering practice during differential current decomposition.

Therefore, the decomposition model considering the sparsity of appliance operation is as follows:

$$f(\boldsymbol{H}) = \|\boldsymbol{I} - \mathbf{A} \bullet \boldsymbol{H}\|_2 + q_1 \|\boldsymbol{H}\|_1 \tag{15}$$

where $q_1$ is the penalty parameter and $q_1 > 0$.

Therefore, the identification of a normal or an arc state in an appliance is transformed into the minimization problem shown in Formula (16):

$$\hat{\boldsymbol{H}} = \arg\min f(\boldsymbol{H}) \tag{16}$$

## 4. Methodology Framework

As shown in Figure 7, the non-intrusive arc fault detection and localization method proposed in this paper, based on the Mann–Kendall Test and current decomposition, includes two stages: the model database construction stage and the identification stage.

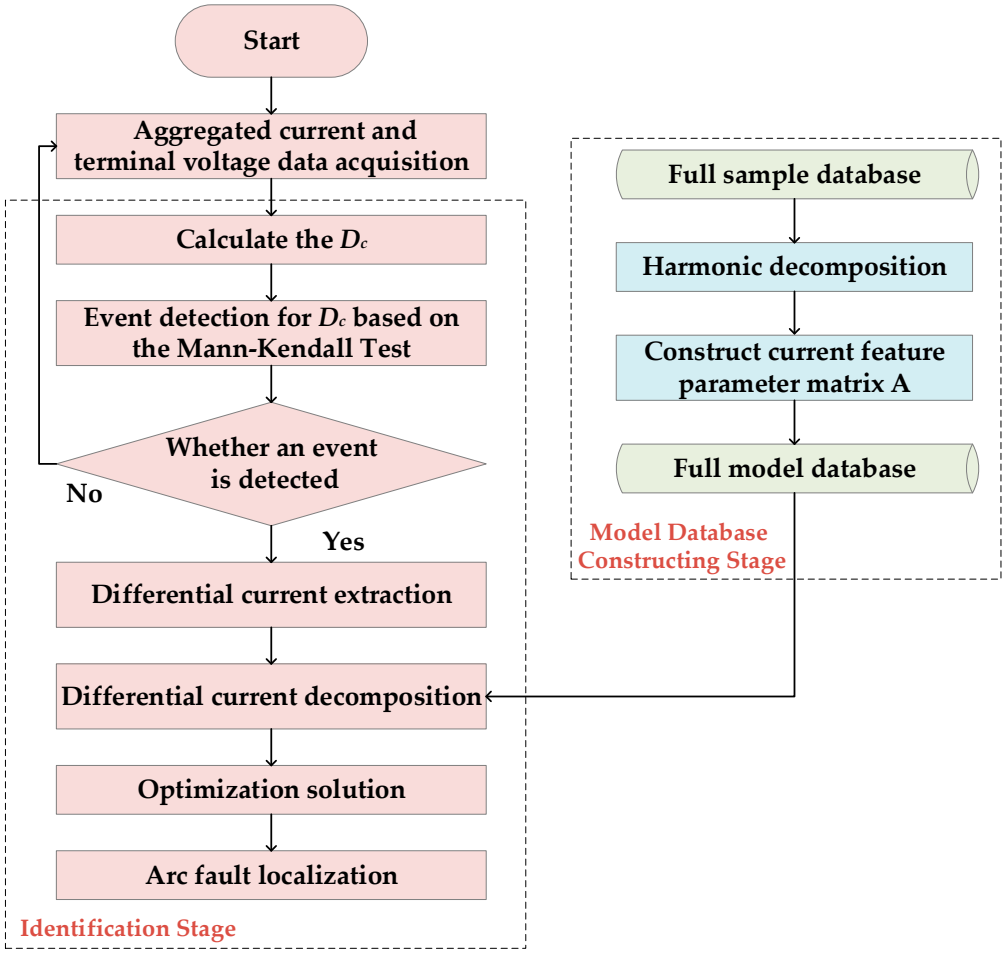



**Figure 7.** Flow chart of the non-intrusive series arc identification and localization method.

In the model database construction stage, a full sample database is constructed by conducting physical arc fault experiments, which includes the current data of each appliance under normal operation and the arc fault operation at a sampling frequency of 25 kHz. Then, Fourier harmonic decomposition is performed on the measured current data of each appliance to extract the key waveform parameters, such as the amplitude and the phase angle of fundamental wave and each of the harmonic waves. Then, the full model database, including the current feature parameter matrix **A** of all the electric appliances under normal operation and the arc fault operation, is obtained for differential current decomposition in the identification stage.

In the identification stage, firstly, the aggregated current and terminal voltage data at the power supply for all appliances is acquired, and then, the $D_c$ of each cycle of aggregated current waveforms is calculated. Next, event detection for $D_c$, based on the Mann–Kendall Test mentioned in Section 2.2., is carried out to find out whether there is an event. If not, we reacquire the aggregated current and terminal voltage data and continue to identify the newly acquired data. If an event is detected, the differential current is obtained by subtracting the current before and after the event, which is mentioned in Section 3.1. Then, harmonic analysis is carried out to obtain the amplitude $\alpha_I$ and phase $\theta_I$ of the aggregated current fundamental wave and each harmonic wave. Next, the matrix

form of the aggregated current $\boldsymbol{I}$ is formed, and the **A** obtained in the model database construction stage is substituted into Equation (15) to form a multi-appliance differential current decomposition model. Then, an intelligent optimization algorithm is used to optimize Equation (16). Finally, the operating state coefficient matrix $\boldsymbol{H}$ of each appliance is obtained, the arc fault can be judged according to the elements in $\boldsymbol{H}$, and the appliance with the arc fault can be located.

## 5. Results and Discussion

In order to verify the effectiveness and accuracy of the low-voltage series arc fault detection and localization method proposed in this paper, an experiment on real measured data was designed. An arc fault generating device was used to generate an arc, and the arc was connected to a simulated low-voltage power line. The simulated residential electrical circuit topology and experimental circuit are shown in Figure 8. The kettle, air conditioner and laptop were, respectively, connected to sockets A, B, and C. The data acquisition device collected the terminal voltage and aggregated current data on the common branch $l_0$ of three appliances.

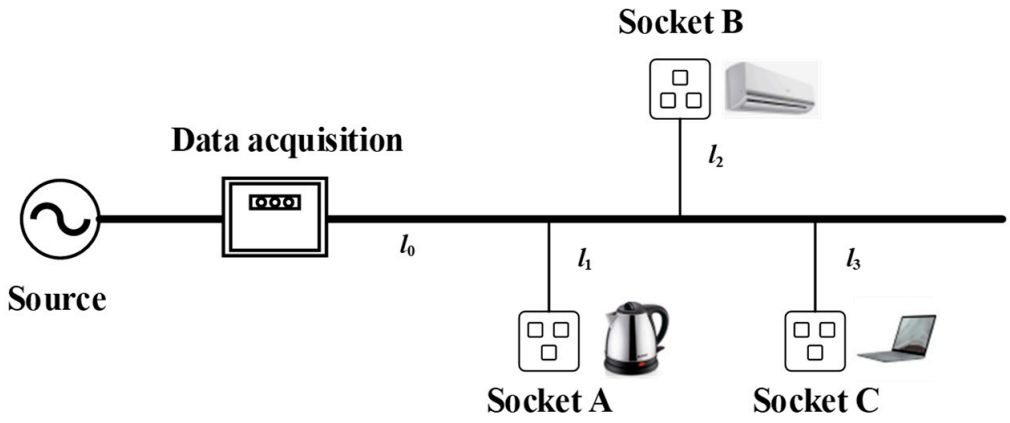



**Figure 8.** Schematic diagram of the experimental scenario.

In this paper, experiments were carried out for different arc fault locations and different appliance operation combinations. The specific experimental design is shown in Table 2. In the experiment, an arc occurred in four lines ($l_0$, $l_1$, $l_2$, and $l_3$). According to Section 2.2, there were two cases of arc events. In the cases of arc events, each arc line and each scenario in which electrical appliances were running constituted a set of experiments, and there were $2 \times 16 = 32$ sets of experiments. Each set of experiments collected 20 s current and voltage datapoints, including data from before and after the arc event. In order to verify the reliability of the proposed method, each set of experiments was repeated 50 times. The experimental data were collected at a sampling frequency of 25,000 Hz in this paper, that is, each current waveform period was composed of 500 sampling points. The frequency of the AC power supply was 50 Hz and the voltage was 220 V. It should be noted that the occurrence of the arc was accompanied by the start event of the electric appliance, so we only needed to detect the start event, and not the stop event; so, in this paper, we only filtered out the timestamp when the start event occurred according to the positive changes in $D_c$.

In order to obtain the current waveform database under normal and arc conditions, the arc-generating device was connected in series with a single appliance, and the arc fault simulation experiment was carried out. The 10 s voltage and current waveform data of each appliance under normal and arc operations were collected to form a full sample database. For the normal and arc currents of each appliance in the sample database, Fourier decomposition was performed to obtain the key waveform parameters and form a current feature parameter matrix **A**.

**Table 2.** Experimental scenario simulation.

| Scenario Number | Arc Position | Appliances |
|---|---|---|
| 1 | $l_0$ | A |
| 2 | | B |
| 3 | | C |
| 4 | | A + B |
| 5 | | A + C |
| 6 | | B + C |
| 7 | | A + B + C |
| 8 | $l_1$ | A + B |
| 9 | | A + C |
| 10 | | A + B + C |
| 11 | $l_2$ | A + B |
| 12 | | B + C |
| 13 | | A + B + C |
| 14 | $l_3$ | A + C |
| 15 | | B + C |
| 16 | | A + B + C |

In order to objectively evaluate the accuracy of the proposed method, this paper used the accurate identification rate of the arc fault ($\gamma$) to evaluate the detection and localization results of the electric appliances with series arcs in each scenario. The formula is as follows:

$$\gamma = \frac{R}{M} \times 100\% \tag{17}$$

where $M$ represents the number of times that the experimental data were collected in each scenario, that is, $M$ = 50 in this paper, and $R$ represents the number of times that each scenario was detected and located correctly.

In the above multiple low-voltage user scenarios, the proposed method is verified. This paper selected the genetic algorithm, which was suitable for dealing with a '0–1' optimization problem to solve the arc detection and localization model. The results of arc detection and localization in each scenario are as shown in Table 3. It can be seen that the accuracy of the proposed method is between 86% and 98% for different arc fault scenarios. Among them, scenario 10 and scenario 16 have the lowest accuracy of 86%. The reason for the low accuracy of arc fault detection and localization in scenario 10 is that when an arc occurs in the kettle, the waveform changes little and the arc features are submerged in the aggregated currents of all the appliances. Additionally, the reason for the low accuracy of arc fault detection and localization in scenario 16 is that sometimes, no event is detected because the arc features are submerged in the currents of the high-power appliances, that is, the kettle or the air conditioner. So, the $D_c$ only changes slightly.

In order to visually display the process and results of arc fault detection and location, for each set of experiments, one of the 50 experimental data acquisitions was randomly selected for further demonstration. The experimental results are presented in Tables 4 and 5. The objective function value (*f-val*) can be used to measure the difference between the fitted differential current and the real differential current. The results of differential current decomposition are represented by numbers. For example, 2 indicates that the air conditioner is under normal working conditions, and 2′ indicates that the air conditioner is in the arc state; the decomposition results of each arc scenario are compared with the ground-truth obtained via pre-labeling. When the arc current result is '1', it indicates that the corresponding appliance is in the arc state. If only one appliance is in the arc state according to the results, the arc fault occurs in the direct power supply branch of the appliance. If multiple appliances are in the arc state according to the results, and other appliances are in normal working condition, the arc fault occurs in the public power supply branch of these appliances. The correct decomposition is marked with 'True'; otherwise, it is marked

with 'False'; *f-val* represents the difference between the fitted differential current and the ground-truth differential current.

**Table 3.** Experimental results of arc fault detection and localization.

| Case | Scenario Number | $\gamma$ | Case | Scenario Number | $\gamma$ |
|---|---|---|---|---|---|
| 1 | 1 | 94% | 2 | 1 | 94% |
| | 2 | 94% | | 2 | 96% |
| | 3 | 92% | | 3 | 92% |
| | 4 | 96% | | 4 | 96% |
| | 5 | 98% | | 5 | 96% |
| | 6 | 94% | | 6 | 94% |
| | 7 | 92% | | 7 | 96% |
| | 8 | 90% | | 8 | 92% |
| | 9 | 92% | | 9 | 90% |
| | 10 | 86% | | 10 | 86% |
| | 11 | 92% | | 11 | 94% |
| | 12 | 94% | | 12 | 92% |
| | 13 | 94% | | 13 | 94% |
| | 14 | 96% | | 14 | 94% |
| | 15 | 92% | | 15 | 94% |
| | 16 | 86% | | 16 | 86% |

**Table 4.** Experimental results of case 1.

| Scenario Number | Decomposition Results | | | | | | Location Results | $f$-Val |
|---|---|---|---|---|---|---|---|---|
| | **1** | **1′** | **2** | **2′** | **3** | **3′** | | |
| 1 | −1 | 1 | 0 | 0 | 0 | 0 | $l_1/l_0$ (True) | 1.58 |
| 2 | 0 | 0 | −1 | 1 | 0 | 0 | $l_2/l_0$ (True) | 1.32 |
| 3 | 0 | 0 | 0 | 0 | −1 | 1 | $l_3/l_0$ (True) | 0.78 |
| 4 | −1 | 1 | −1 | 1 | 0 | 0 | $l_0$ (True) | 2.96 |
| 5 | −1 | 1 | 0 | 0 | −1 | 1 | $l_0$ (True) | 0.47 |
| 6 | 0 | 0 | −1 | 1 | −1 | 1 | $l_0$ (True) | 0.86 |
| 7 | −1 | 1 | −1 | 1 | −1 | 1 | $l_0$ (True) | 1.53 |
| 8 | −1 | 1 | 0 | 0 | 0 | 0 | $l_1$ (True) | 2.67 |
| 9 | −1 | 1 | 0 | 0 | 1 | 0 | $l_1$ (True) | 2.48 |
| 10 | 0 | 0 | 0 | 0 | 0 | 0 | None (False) | None |
| 11 | 0 | 0 | −1 | 1 | 0 | 0 | $l_2$ (True) | 1.62 |
| 12 | 0 | 0 | −1 | 1 | 0 | 0 | $l_2$ (True) | 0.78 |
| 13 | 0 | 0 | −1 | 1 | 0 | 0 | $l_2$ (True) | 1.41 |
| 14 | 0 | 0 | 0 | 0 | −1 | 1 | $l_3$ (True) | 1.16 |
| 15 | 0 | 0 | 0 | 0 | −1 | 1 | $l_3$ (True) | 1.95 |
| 16 | 0 | 0 | 0 | 0 | 0 | 0 | None (False) | None |

**Table 5.** Experimental results of case 2.

| Scenario Number | Decomposition Results | | | | | | Location Results | $f$-Val |
|---|---|---|---|---|---|---|---|---|
| | **1** | **1′** | **2** | **2′** | **3** | **3′** | | |
| 1 | 0 | 1 | 0 | 0 | 0 | 0 | $l_1/l_0$ (True) | 1.32 |
| 2 | 0 | 0 | 0 | 1 | 0 | 0 | $l_2/l_0$ (True) | 0.91 |
| 3 | 0 | 0 | 0 | 0 | 0 | 1 | $l_3/l_0$ (True) | 0.86 |
| 4 | 0 | 1 | 0 | 1 | 0 | 0 | $l_0$ (True) | 2.85 |
| 5 | 0 | 1 | 0 | 0 | 0 | 1 | $l_0$ (True) | 0.46 |
| 6 | 0 | 0 | 0 | 1 | 0 | 1 | $l_0$ (True) | 0.77 |
| 7 | 0 | 1 | 0 | 1 | 0 | 1 | $l_0$ (True) | 1.47 |
| 8 | 0 | 1 | 1 | 0 | 0 | 0 | $l_1$ (True) | 3.12 |

**Table 5.** *Cont.*

| Scenario Number | Decomposition Results | | | | | | Location Results | $f$-Val |
|---|---|---|---|---|---|---|---|---|
| | **1** | **1′** | **2** | **2′** | **3** | **3′** | | |
| 9 | 0 | 1 | 0 | 0 | 1 | 0 | $l_1$ (True) | 2.77 |
| 10 | 0 | 1 | 1 | 0 | 0 | 1 | $l_0$ (False) | 4.65 |
| 11 | 1 | 0 | 0 | 1 | 0 | 0 | $l_2$ (True) | 1.21 |
| 12 | 0 | 0 | 0 | 1 | 1 | 0 | $l_2$ (True) | 0.88 |
| 13 | 1 | 0 | 0 | 1 | 1 | 0 | $l_2$ (True) | 1.51 |
| 14 | 1 | 0 | 0 | 0 | 0 | 1 | $l_3$ (True) | 0.98 |
| 15 | 0 | 0 | 1 | 0 | 0 | 1 | $l_3$ (True) | 2.02 |
| 16 | 0 | 1 | 1 | 0 | 1 | 0 | $l_1$ (False) | 3.45 |

## 6. Conclusions

The accurate detection and localization of arc faults can eliminate the hidden danger of electricity in time, which is of great significance for protecting people 's lives and property. Non-intrusive arc fault detection and localization only requires the acquisition of aggregated currents at the power supply entrance, which provides the possibility for the large-scale application of arc fault detection. To this end, this paper proposes a novel non-intrusive arc fault detection and location method based on the Mann–Kendall Test and differential current decomposition.

Firstly, the arc current waveforms of different appliances are obtained using an arc fault generator, and the common arc current characteristics are analyzed. Then, in order to achieve non-intrusive arc detection and localization, we use the Mann–Kendall Test to detect the aggregated current. After the event is detected, in order to extract the current of the electric appliances that caused the event, the current waveforms before and after the event are subtracted after their voltage phases are aligned. Based on the current decomposition model proposed in this paper, the arc fault detection and localization problem is transformed into an optimization problem using harmonic decomposition. The method of decomposing the differential current proposed in this paper can effectively detect and locate the arc fault, even if multiple electric appliances are turned on at the same time, and improve calculation efficiency. By solving the optimization problem, the appliances in series with the arc can be identified. Finally, the experimental results show that the proposed method has high accuracy for series arc fault detection and localization. In the future, we will collect the arc data of more electric appliances and construct a more comprehensive model database to further verify the applicability of the proposed method. In addition, the current decomposition optimization method will be further studied to improve the accuracy of the proposed method and reduce the response time.

**Author Contributions:** Conceptualization, B.L.; data curation, Z.Y., H.C., X.L. and D.X.; funding acquisition, W.J. and B.L.; investigation, Z.Y., H.C. and X.L.; methodology, W.J. and B.L.; project administration, W.J., Z.Y. and X.L.; resources, W.J. and X.L.; software, W.J. and H.C.; validation, W.J., Z.Y., H.C. and D.X.; visualization, D.X.; writing—original draft, B.L. and H.C.; writing—review and editing, B.L. All authors have read and agreed to the published version of the manuscript.

**Funding:** This research was supported by the Science and Technology Projects of Guangxi Power Grid Corporation (No. 044400KK52200003) and the National Natural Science Foundation for Young Scholars of China (No. 52107120).

**Data Availability Statement:** Not applicable.

**Conflicts of Interest:** The authors declare no conflict of interest.

## References


1. Fire Department of Ministry of Public Security. *2016 China Fire Yearbook*; People's Publishing House: Kunming, China, 2016.
2. General Administration of Quality Supervision, Inspection and Quarantine of the People's Republic of China; Standardization Administration of the People's Republic of China. *Electrical Fire Monitoring System–Part 4: Arcing Fault Detectors (GB14287.4-2014)*; Standards Press of China: Beijing, China, 2014.
3. George, D.G.; Gary, W.S. The arc-fault circuit interrupter: An emerging product. *IEEE Trans. Ind. Appl.* **1998**, *34*, 928–933.
4. Zhan, Y.X.; Zhang, R.C.; Yang, J.H. Fault Diagnosis Method of Series Arc Based on Camberra Distance. *Power Syst. Prot. Control* **2014**, *12*, 30–36.
5. Restrepo, C.E. Arc Fault Detection and Discrimination Methods. In Proceedings of the 53rd IEEE Holm Conference on Electrical Contacts, Pittsburgh, PA, USA, 16–19 September 2007; pp. 115–122.
6. Abdullah, Y.; Hu, B.; Wei, Z. Adaptive detection of DC Arc faults based on hurst exponents and current envelope. In Proceedings of the 2018 IEEE Applied Power Electronics Conference and Exposition, San Antonio, TX, USA, 4–8 March 2018; pp. 3392–3397.
7. Yu, Q.F.; Hu, Y.Q.; Yang, Y. Identification Method for Series Arc Faults Based on Wavelet Transform and Deep Neural Network. *Energies* **2020**, *13*, 142. [CrossRef]
8. Cassie, A.M. Theorie Nouvelle des Arcs de Rupture et de la Rigidité des Circuits. *Cigre* **1939**, *102*, 588–608.
9. Mayr, O. Beitrage zur Theorie des Statischen und des Dynamischen Lichthogens. *Arch. Elktrotech.* **1943**, *37*, 588–608. [CrossRef]
10. Habedank, U. Application of a new arc model for the evaluation of short-circuit breaking tests. *IEEE Trans. Power Deliv.* **1993**, *8*, 1921–1925. [CrossRef]
11. Schavemaker, P.H.; van der Slui, L. An improved Mayr-type arc model based on current-zero measurements. *IEEE Trans. Power Deliv.* **2000**, *15*, 580–584. [CrossRef]
12. Guardado, J.L.; Maximov, S.G.; Melgoza, E.; Naredo, J.L.; Moreno, P. An improved arc model before current zero based on the combined Mayr and Cassie arc models. *IEEE Trans. Power Deliv.* **2005**, *20*, 138–142. [CrossRef]
13. Golestani, S.; Samet, H. Generalised Cassie–Mayr electric arc furnace models. *IET Gener. Transm. Distrib.* **2016**, *10*, 3364–3373. [CrossRef]
14. Wang, Q.L.; Wang, B.W.; Guan, H.L. Model and experiment of low voltage AC series fault arc. *J. Electr. Power Syst. Autom.* **2018**, *30*, 26–30.
15. Jalil, M.; Samet, H.; Ghanbari, T.; Tajdinian, M. An Enhanced Cassie–Mayr-Based Approach for DC Series Arc Modeling in PV Systems. *IEEE Trans. Instream. Meas.* **2021**, *70*, 1–10. [CrossRef]
16. Kay, J.A.; Kumpulainen, L. Maximizing Protection by Minimizing Arcing Times in Medium-Voltage Systems. *IEEE Trans. Ind. Appl.* **2013**, *49*, 1920–1927. [CrossRef]
17. Parikh, P.; Allcock, D.; Luna, R.; Vico, J. A Novel Approach for Arc-Flash Detection and Mitigation: At the Speed of Light and Sound. *IEEE Trans. Ind. Appl.* **2014**, *50*, 1496–1502. [CrossRef]
18. Ke, Y.; Zhang, W.; Suo, C.; Wang, Y.; Ren, Y. Research on Low-Voltage AC Series Arc-Fault Detection Method Based on Electromagnetic Radiation Characteristics. *Energies* **2022**, *15*, 1829. [CrossRef]
19. Zhao, H.; Liu, J.; Lou, J. Series arc fault detection based on current fluctuation and zero-current features. *Electr. Power Syst. Res.* **2022**, *202*, 107626. [CrossRef]
20. Lezama, J.; Schweitzer, P.; Tisserand, E.; Humbert, J.; Weber, S.; Joyeux, P. An embedded system for AC series arc detection by inter-period correlations of current. *Electr. Power Syst. Res.* **2015**, *129*, 227–234. [CrossRef]
21. Qu, N.; Zuo, J.; Chen, J.; Li, Z. Series Arc Fault Detection of Indoor Power Distribution System Based on LVQ-NN and PSO-SVM. *IEEE Access* **2019**, *7*, 184020–184028. [CrossRef]
22. Qu, N.; Wang, J.; Liu, J. An Arc Fault Detection Method Based on Current Amplitude Spectrum and Sparse Representation. *IEEE Trans. Instrum. Meas.* **2019**, *68*, 3785–3792. [CrossRef]
23. Kim, J.C.; Neacşu, D.O.; Ball, R.; Lehman, B. Clearing Series AC Arc Faults and Avoiding False Alarms Using Only Voltage Waveforms. *IEEE Trans. Power Deliv.* **2020**, *35*, 946–956. [CrossRef]
24. Wang, Y.; Zhang, F.; Zhang, S. A New Methodology for Identifying Arc Fault by Sparse Representation and Neural Network. *IEEE Trans. Instrum. Meas.* **2018**, *67*, 2526–2537. [CrossRef]
25. Yang, J.H.; Fang, H.Y.; Zhang, R.C.; Yang, K. An arc fault diagnosis algorithm using multiinformation fusion and support vector machines. *R. Soc. Open Sci.* **2018**, *5*, 180160. [CrossRef] [PubMed]
26. Wang, Y.; Hou, L.; Paul, K.C.; Ban, Y.; Chen, C.; Zhao, T. ArcNet: Series AC Arc Fault Detection Based on Raw Current and Convolutional Neural Network. *IEEE Trans. Ind. Inform.* **2022**, *18*, 77–86. [CrossRef]
27. Li, W.; Liu, Y.; Li, Y.; Gao, F. Series Arc Fault Diagnosis and Line Selection Method Based on Recurrent Neural Network. *IEEE Access* **2020**, *8*, 177815–177822. [CrossRef]
28. Jiang, J.; Li, W.; Wen, Z.; Bie, Y.; Schwarz, H.; Zhang, C. Series Arc Fault Detection Based on Random Forest and Deep Neural Network. *IEEE Sens. J.* **2021**, *21*, 17171–17179. [CrossRef]
29. Qu, N.; Wang, J.H.; Liu, J.H. An arc fault detection method based on multidictionary learning. *Math. Probl. Eng.* **2018**, *2018*, 1–8. [CrossRef]
30. Artale, G.; Cataliotti, A.; Cosentino, V.; Cara, D.D.; Nuccio, S.; Tinè, G. Arc Fault Detection Method Based on CZT Low-Frequency Harmonic Current Analysis. *IEEE Trans. Instrum. Meas.* **2017**, *66*, 888–896. [CrossRef]

31. Wang, Z.; Balog, R.S. Arc Fault and Flash Signal Analysis in DC Distribution Systems Using Wavelet Transformation. *IEEE Trans. Smart Grid.* **2015**, *6*, 1955–1963. [CrossRef]
32. Miao, W.; Xu, Q.; Lam, K.H.; Pong, P.W.T.; Poor, H.V. DC Arc-Fault Detection Based on Empirical Mode Decomposition of Arc Signatures and Support Vector Machine. *IEEE Sens. J.* **2021**, *21*, 7024–7033. [CrossRef]
33. Lin, J.; Luan, W.; Liu, B. A Novel Non-Intrusive Arc Fault Detection Method for Low-Voltage Customers. In Proceedings of the 6th Asia Conference on Power and Electrical Engineering (ACPEE), Chongqing, China, 8–11 April 2021; pp. 84–88.
34. Luan, W.; Lin, J.; Liu, B.; Zhao, B. Arc fault detection and identification via non-intrusive current disaggregation. *Electr. Power Syst. Res.* **2022**, *210*, 108113. [CrossRef]
35. Dowalla, K.; Bilski, P.; Łukaszewski, R.; Wójcik, A.; Kowalik, R. A Novel Method for Detection and Location of Series Arc Fault for Non-Intrusive Load Monitoring. *Energies* **2023**, *16*, 171. [CrossRef]
36. *Safety for Arc-Fault Circuit-Interrupters*; Underwriter Laboratories Inc.: Northbrook, IL, USA, 2008.
37. Liu, Z.; Cao, X.; Wang, Z.; Li, J.; Chen, X. Non-invasive electric arc fault detection based on sliding approximate entropy. In Proceedings of the 5th International Workshop on Advanced Algorithms and Control Engineering, Zhuhai, China, 26–28 February 2021; p. 012102.
38. Gocic, M.; Trajkovic, S. Analysis of changes in meteorological variables using Mann-Kendall and Sen's slope estimator statistical tests in Serbia. *Glob. Planet. Chang.* **2013**, *100*, 172–182. [CrossRef]


**Disclaimer/Publisher's Note:** The statements, opinions and data contained in all publications are solely those of the individual author(s) and contributor(s) and not of MDPI and/or the editor(s). MDPI and/or the editor(s) disclaim responsibility for any injury to people or property resulting from any ideas, methods, instructions or products referred to in the content.